metals

MDPI

Article

Simultaneous Improvement in Strength and Ductility of TC4 Matrix Composites Reinforced with Ti1400 Alloy and In Situ-Synthesized TiC

Ni He [1], Mingjia Li [2,*], Guodong Sun [2], Junjie Xu [2], Mingyang Li [2], Longlong Dong [3] and Yusheng Zhang [1,3]

[1] School of Materials Science and Engineering, Northeastern University, Shenyang 110819, China; hn1239210639@163.com (N.H.)
[2] Xi'an Rare Metal Materials Institute Co., Ltd., Xi'an 710075, China
[3] Advanced Materials Research Central, Northwest Institute for Nonferrous Metal Research, Xi'an 710016, China
* Correspondence: mjli0113@163.com

Abstract: To overcome the tradeoff between strength and ductility of materials and obtain titanium matrix composites with excellent mechanical properties, in this study, the in situ-synthesized TiC particles and Ti-Al-V-Mo-Cr (Ti1400) alloy-reinforced Ti6Al4V (TC4) matrix composites ((Ti1400 + TiC)/TC4) were fabricated by low-energy ball milling and spark plasma sintering. The inhomogeneous distribution of TiC particles and Ti1400 alloy, as well as the compositional and structural transition zone, were characterized. The TiC/TC4 composite displayed a significantly higher yield strength and tensile strength compared to the TC4 alloy. However, the total elongation of the TiC/TC4 composite was only 57% of that in the TC4 alloy. In contrast, the (Ti1400 + TiC)/TC4 composites exhibited noticeably higher total elongation than the TiC/TC4 composite. Furthermore, the tensile strength of the composite increased with the increase in Ti1400 alloy content. The increase in strength can be attributed to solid solution strengthening and fine grain strengthening. The compositional and structural transition zone, formed by element diffusion, provided a better interface combination between the reinforcements and TC4 matrix. In the transition zone and Ti1400 region, a large number of α/β interfaces can effectively alleviate the stress concentration, and the increase in the β phase can bear more plastic deformation, which is conducive to improving the elongation of the composite. As a result, the (Ti1400 + TiC)/TC4 composites exhibited simultaneous improvements in strength and ductility.

Keywords: titanium matrix composites; mechanical properties; in situ synthesis; powder metallurgy; strengthening mechanism

Citation: He, N.; Li, M.; Sun, G.; Xu, J.; Li, M.; Dong, L.; Zhang, Y. Simultaneous Improvement in Strength and Ductility of TC4 Matrix Composites Reinforced with Ti1400 Alloy and In Situ-Synthesized TiC. *Metals* **2023**, *13*, 965. https://doi.org/10.3390/met13050965

Academic Editor: Daria Lazurenko

Received: 11 April 2023
Revised: 12 May 2023
Accepted: 15 May 2023
Published: 16 May 2023

1. Introduction

Titanium matrix composites (TMCs) are a promising material in aerospace, biomedicine, and automotive industries. By adding reinforcements to titanium and its alloys, TMCs possess ultra-high specific strength, low density, exceptional corrosion resistance, and high temperature resistance [1–7]. TMCs can be categorized into two types: continuously reinforced titanium matrix composites (CRTMCs) that utilize continuous fibers such as SiC, C, B, and Al_2O_3 as reinforcements, and discontinuously reinforced titanium matrix composites (DRTMCs) that employ whiskers and particles such as TiB and TiC as reinforcements. While CRTMCs possess exceptional properties such as high strength, high temperature resistance, and creep resistance, they also have drawbacks such as processing difficulties and anisotropic mechanical properties. Additionally, the weak interfacial bond strength between reinforcement and matrix makes CRTMCs prone to cracking under stress, which hinders their further development. As a result, DRTMCs have garnered significant attention in recent years because they can be flexibly designed in terms of composition

and structure and can be fabricated in various ways to meet the service requirements of different application environments.

The majority of research efforts have focused on selecting reinforcements, investigating the microstructure, and evaluating the mechanical properties of DRTMCs. A range of ceramic reinforcements, such as TiB, TiC, TiN, B_4C, and Ti_5Si_3, are commonly utilized to reinforce Ti alloys for the production of TMCs with superior properties [8–21]. In addition, carbon nanoparticles and graphene are also promising reinforcements due to their low density and high modulus, making TMCs suitable for weight reduction and strengthening purposes in the aerospace and automotive industries, but graphene has disadvantages such as easy agglomeration and difficult dispersion due to its high activity [5,8,22–24]. However, for conventional TMCs, the pursuit of super high strength often requires increasing the reinforcement content, which can significantly compromise the ductility of TMCs [8,19,21]. Based on the mechanical properties of TMCs reported thus far, the elongation of TMCs with tensile strength exceeding 1200 MPa is typically less than 10% (indicating good tensile ductility). To improve the ductility of composite materials, interfacial bonding and stress distribution can be enhanced. The severe blockage of dislocations and weak interfacial bonding between reinforcements and matrix result in stress concentration around the reinforcements, which inevitably reduces ductility. Therefore, effective techniques for improving the plasticity of TMCs include enhancing interfacial bonding and ensuring uniform stress distribution.

Incorporating reinforcements into the matrix to enhance interface bonding can reduce the significant discrepancy in mechanical–physical properties between the matrix and reinforcements, while avoiding the sacrifice of plasticity. Cho et al. [25] fabricated TiC-reinforced Fe-0.2C-7Mn composites (TiC/Fe-0.2C-7Mn) with molybdenum (Mo). The mechanical strength of the TiC/Fe-0.2C-7Mn composite was significantly improved with the addition of Mo atoms, which can be attributed to the considerably enhanced strength of the interface caused by Mo migration. Composite materials were prepared using two types of metals or alloys with similar crystal structures, enabling the formation of a coherent lattice relationship and better interfacial bonding through component diffusion, thus contributing to improved mechanical properties [26–28]. Luo et al. [29] reinforced AZ91 magnesium matrix composites with Ti6Al4V (TC4), which showed increased tensile strength and elongation compared to an AZ91 alloy. The improvement of mechanical properties can be attributed to the strong interfacial bonding between the Mg matrix and TC4 particles through the formation of coherent interfacial bonding. Meanwhile, TC4 particles can relieve the stress concentration, and the composites can achieve comprehensive mechanical properties with high strength and excellent plasticity. Xiong et al. [30] obtained good overall performance with a strength of 1150 MPa and elongation of 8.8% by using high-entropy alloy-reinforced titanium matrix composites. This is mainly due to the mutual diffusion between the high-entropy alloy and the titanium matrix to form a diffusion layer, which produces reinforcement. However, similar studies are rarely observed in titanium matrix composites.

This study utilized TC4 alloy, a widely available α+β-type titanium alloy, and TiC as the matrix and reinforcement, respectively, to prepare TiC/TC4 composites. TiC has high strength, stiffness, and wear resistance as well as a similar linear expansion coefficient, density, and Poisson's ratio to titanium alloy. It can be better integrated with the matrix and mitigate the damage to the composite material caused by the incompatibility between the reinforcement and the matrix [31]. Ti1400 alloy, a near β-type titanium alloy, was also employed. The α and β phases, which possess the same crystal structure as the stable phase of TC4 alloy at room temperature, can be obtained through gradual cooling from the high temperature β-phase region. The similar crystal structure enables Ti1400 alloy and TC4 alloy to have excellent interface bonding, which enhances ductility. The β-stabilizing elements, Vanadium (V), Molybdenum (Mo), and Chromium (Cr) present in Ti1400 alloy, can form a continuous solid solution in the β phase of TiC/TC4 composites and Ti1400 alloy, resulting in a superior interfacial bond and increased room-temperature strength via solid

solution strengthening [32,33]. (Ti1400 + TiC)/TC4 composites were fabricated through a low-energy ball milling and spark plasma sintering (SPS) method [16,34,35]. The scanning electron microscope, electron probe, and TEM were used to analyze the inhomogeneous distribution of compositions and reinforcements. Furthermore, the interface properties and strengthening mechanism of the composites with Ti1400 alloy were investigated.

2. Materials and Methods

2.1. Material Preparation

Figure 1 illustrates the process of fabricating (Ti1400 + TiC)/TC4 composites. The morphologies of TC4 powders (15–53 µm with 99.9% purity, Sino-Euro materials technologies of Xi' an Co., Ltd., Xi'an, China), carbon nanoparticles (CNPs) (20 nm, purity ≥99.8%, Shaanxi Coal and Chemical Industry Group Co., Ltd., Xi'an, China), and Ti1400 powders (15–53 µm with 99.9% purity, Sino-Euro materials technologies of Xi' an Co., Ltd., Xi'an, China) are displayed in Figure 1a–c, respectively. It can be seen that both TC4 and Ti1400 powders are spherical and uniform in size.

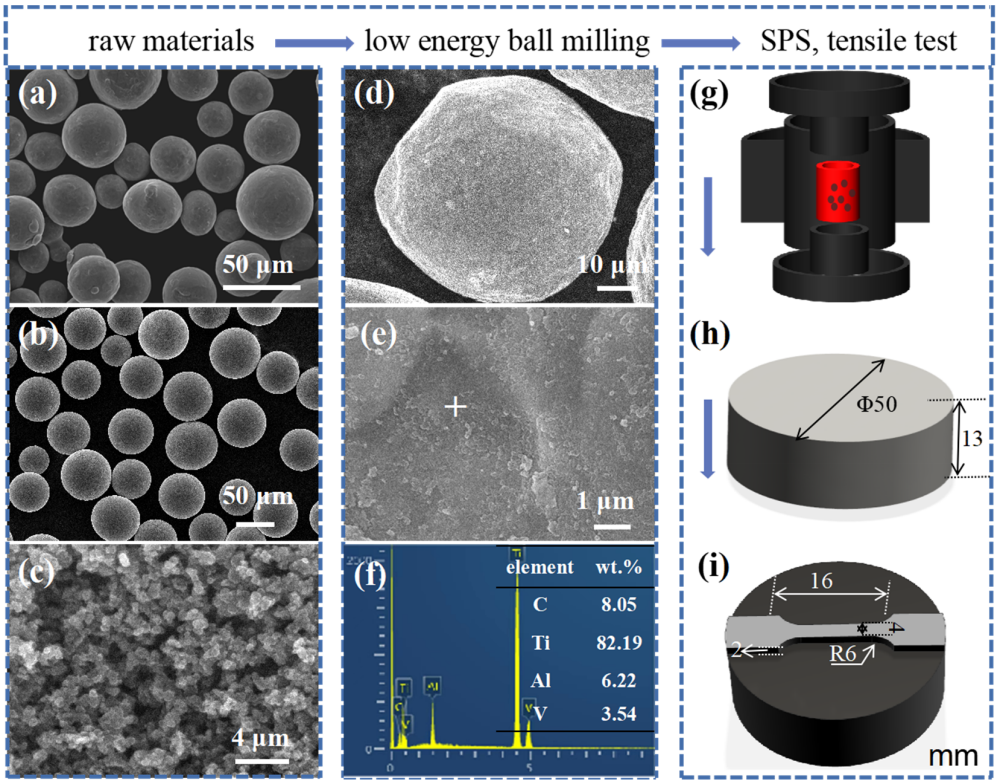

Figure 1. Fabrication processes of TC4 alloy and composites. SEM images of (**a**) the raw TC4 powders, (**b**) Ti1400 powders, (**c**) CNP powders, (**d**,**e**) raw powders after LEM, (**f**) EDS at the marker (+) in (**e**), (**g**) SPS sintering of mixed powders, (**h**) the block schematic after sintering, (**i**) dimensions of tensile sample.

Table 1 shows the compositions of TC4 and Ti1400 powders. To achieve an inhomogeneous distribution of compositions and reinforcements, spherical TC4 powders with CNPs and spherical Ti1400 powders were subjected to low-energy ball milling (LEM) for 5 h at a speed of 200 rpm (the ball-to-powder weight ratio was 6:1).

Table 1. The compositions of the raw TC4 alloy and Ti1400 alloy powders.

Element (w/t)	Al	V	Fe	Cr	Mo	Sn	Zr
TC4	6.07	3.93	0.18	/	/	/	/
Ti1400	4.12	4.62	0.18	5.55	4.16	<0.01	<0.01

Figure 1d–f depict the morphology and composition of powders after LEM, indicating that CNPs were uniformly embedded on the surface of TC4 powders. The mixed powders were sintered via SPS at 1273 K for 5 min under a pressure of 40 MPa, as shown in Figure 1g. During the sintering process, the vacuum degree was maintained at 10^{-2} Pa to prevent excessive oxygen and hydrogen from deteriorating the mechanical properties of TMCs [36,37]. After sintering, trace amounts of oxygen and hydrogen would dissolve in TMCs as interstitial solid solutions, which can strengthen the matrix [38]. Additionally, the TiC particles can be in situ-synthesized according to Equation (1).

$$\text{Ti (s)} + \text{C (s)} \rightarrow \text{TiC (s)} \quad (1)$$

Figure 1h displays the dimensions of the cylindrical composite, which are ϕ50 mm × 13 mm. To facilitate comparison analysis, composites with different Ti1400 weight fractions (0 wt.%, 5 wt.%, and 20 wt.%) and 2.5 wt.% TiC were designed and prepared using the same preparation process, along with the monolithic TC4 alloy. These samples were named TC4, TMC-0 (2.5%TiC/TC4), TMC-5 ((5%Ti1400 + 2.5%TiC)/TC4), and TMC-20 ((20%Ti1400 + 2.5%TiC)/TC4), respectively.

2.2. Material Characterization

The polished samples were etched using etching solution, which was prepared by hydrofluoric acid, nitric acid, and distilled water, with a volume fraction ratio of 2:3:100, and then observed with a cold field emission scanning electron microscope (JSM-7500F produced by Nippon Tsunen Industrial (Hong Kong) Co., Ltd.). X-ray diffraction (XRD) analysis was conducted using an RU-300 diffractometer with Cu radiation, operating at 40 kV and 40 mA, to identify the phases. The element distribution of the samples was characterized by an electron probe X-ray microanalyzer (EPMA). Electron backscatter diffraction (EBSD) observations were performed on a scanning electron microscope (SEM) (SU3500, Hitachi, Japan) equipped with an AZtec 3.0 EBSD system. The electron beam was moved in 0.5 μm steps in a 200 × 200 μm area. The specimens were mechanically ground to 0.5 μm and then electropolished in solution consisting of 6% $HClO_4$/34% $CH_3(CH_2)_3OH$/60% CH_3OH at a voltage of 35 V for 25 s. Transmission electron microscope (TEM) observations were performed on a Talos F200S system operated at 200 kV. The samples used to measure tensile properties were cut from the cylindrical composite using an electron discharge machine with a parallel section length, width, and thickness of 16 mm, 4 mm, and 2 mm, respectively, as illustrated in Figure 1i. The tensile test was performed on a UTM5105X type electronic universal testing machine with a load force of 100 KN at a speed of 1 mm/min. The tensile test was repeated 4 times. The mean and error were calculated and plotted.

3. Results

Figure 2 displays the SEM images and EDS mappings of TMC-20 powders after ELM. Figure 2a illustrates that the shape and size of the spherical powders remained relatively unchanged. In the high magnification image of Figure 2b, the surface of the powders exhibited slight evidence of collision and had many small particles of CNPs attached. The Energy Dispersive Spectroscopy (EDS) images in Figure 2c–h revealed that Ti, Al, V, and C were detected in all four spherical powders in Figure 2b, indicating that the CNPs were uniformly attached to the powder surface. Cr and Mo were detected in the two powders, which suggests that these are Ti1400 powders, as shown in Figure 2g,h.

Figure 3 illustrates the XRD patterns of the TC4 alloy and the composites with varying Ti1400 alloy contents. Peaks corresponding to hexagonal close-packed (HCP) α phase and body-centered cubic (BCC) β phase can be detected in the TC4 alloy, TMC-0, TMC-5, and TMC-20 composites. The intensity of the β-phase diffraction peak gradually increased with the addition of Ti1400 alloy. There are two weak peaks of TiC, corresponding to its (111) plane and (200) plane, which were present in the TMC-0, TMC-5, and TMC-20 samples. This shows that CNPs react with Ti to form TiC.

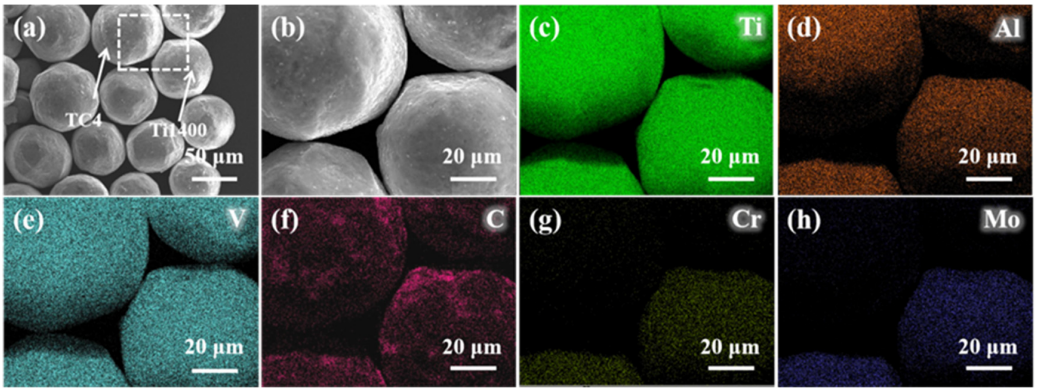

Figure 2. (**a**) SEM image of raw powders after LEM, (**b**) magnification SEM image of the square area in (**a**), (**c**–**h**) EDS mappings of Ti, Al, V, C, Cr, and Mo.

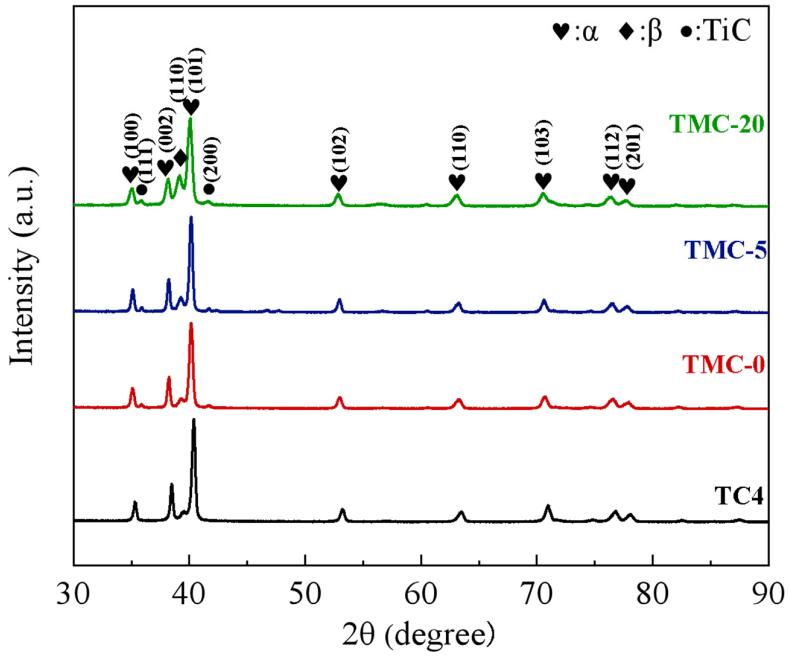

Figure 3. XRD profiles of TC4 alloy and the composites with different Ti1400 alloy contents.

Figure 4 displays the SEM images of the TC4 alloy, TMC-0, TMC-5, and TMC-20. Figure 4a highlights the typical Widmannstatten structure of the TC4 alloy, consisting of lamellar α phase and β phase, with the thicker α phase present at the grain boundary of the primary β phase. Figure 4b illustrates that the in situ reaction produced TiC particles of around 2 μm, which were discontinuously distributed around the TiC-lean region to form a 3D network structure. The size of the network unit was similar to the diameter of the raw spherical TC4 powder. Within the network unit, the length of lamellar structures was significantly shorter than that of the TC4 alloy. The 3D network structure of TiC and the inhomogeneous distribution of Ti1400 alloy in TMC-5 and TMC-20 are depicted in Figure 4c–f. Macroscopically, the β phase formed by Ti1400 and the α+β phase formed by TC4 were uniformly distributed, and the β phase increased with the increase in Ti1400 content. Microscopically, TC4 showed equiaxed biphasic organization, Ti1400 showed an elongated needle-like β phase, and a transition zone was formed between TC4 and Ti1400, regarding the determination of the transition zone. The transition zone between the white dashed lines in Figure 4f was determined based on the particle size of the original powders of TC4 alloy and Ti1400 alloy, and its approximate range was defined accordingly. The average size of TC4 alloy and Ti1400 alloy powders was 31.10 μm and 50.37 μm, respectively. After sintering, the TC4 matrix surrounded by TiC particles was approximately 30 μm,

which was not significantly different from the original powder size. The Ti1400 area was approximately 90 μm, which was significantly larger than its original powder size. The enlargement of the Ti1400 area was caused by the diffusion of Cr and Mo elements into the TC4 matrix. Therefore, the area larger than the original Ti1400 powder size was considered as the transition zone between Ti1400 alloy and TC4 matrix. Additionally, it can be found that the β phase gradually becomes shorter and wider from Ti1400 to the transition zone, which is related to the element diffusion and will be discussed in detail later. It can be seen from Figure 4e,f that TiC particles were not distributed around the Ti1400 region but were mainly distributed in the TC4 matrix and the transition zone.

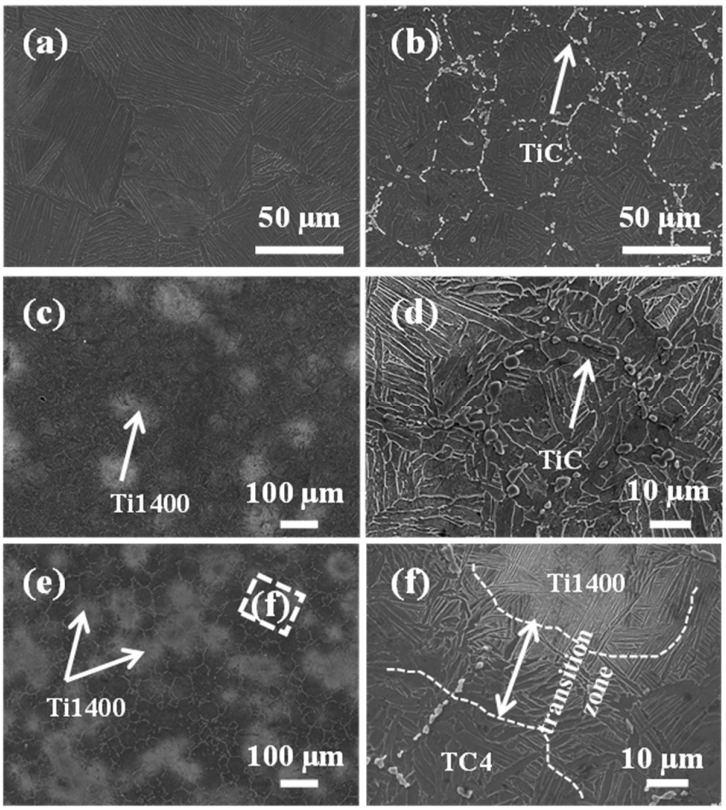

Figure 4. SEM images of (**a**) TC4 alloy, (**b**) TMC-0, (**c**,**d**) TMC-5, and (**e**,**f**) TMC-20.

Figure 5 displays the elemental distribution of Al, V, Cr, Mo, and C in TMC-0 and TMC-20, respectively. Figure 5a shows a network unit and its lamellar structures in TMC-0. The C in the form of TiC is mainly distributed in the network unit surrounding the raw spherical TC4 powder. Within the lamellar structures, Al and V, serving as the α-stabilizing and β-stabilizing elements, respectively, were alternately distributed in the lamellar layers of the α phase and β phase, as depicted in Figure 5(a_1–a_3). The network unit of particles surrounding the raw spherical Ti1400 powder and the distribution of C in TMC-20 were similar with those in TMC-0 (Figure 5b(b_1)). The contents of Al and V within the region of Ti1400 were lower than those in the TC4 matrix. Cr and Mo were mainly distributed in Ti1400 region, with a small amount diffusing into the TC4 matrix, of which Cr diffused more than Mo [39], as shown in Figure 5(b_2–b_5). At the sintering temperature of 1000 °C, the diffusion coefficient of Cr is greater than that of Mo, resulting in Cr diffusing more easily to the surroundings than Mo [39]. Meanwhile, Cr and Mo are β-stabilizing elements and can promote the formation of the β phase, which explains the formation of the transition zone between Ti1400 and TC4. Closer to the TC4 matrix, the β phase becomes shorter and wider.

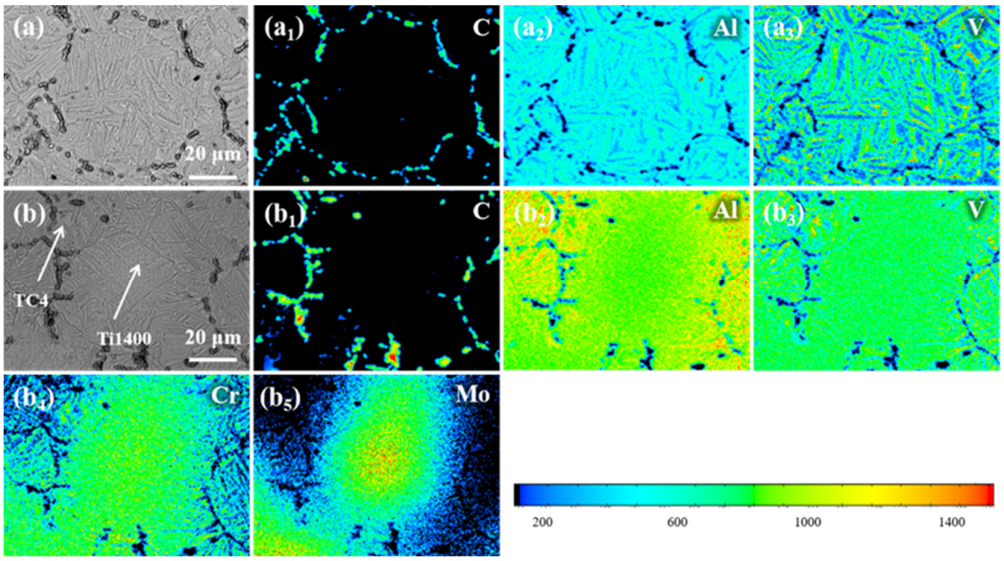

Figure 5. EPMA images of (**a**–**a$_3$**) TMC-0 and (**b**–**b$_5$**) TMC-20.

Figure 6 illustrates the structures and compositions of the α phase, β phase, and TiC particles present in TMC-20. In the bright-field image of Figure 6a, lamellar structures and nearly circular particles were observed. The selected area electron diffraction (SAED) patterns shown in Figure 6b,c, taken from the white circle region in Figure 6a, revealed spots of α phase, β phase, and TiC along the $[0001]_\alpha$ zone axis, $[531]_\beta$ zone axis, and $[1\bar{2}1]_\beta$ zone axis, respectively. The EDS images in Figure 6d–i displayed the compositions of TiC in the square area of Figure 6a, where particles approximately 1 μm in size were mainly composed of C and Ti elements. Additionally, the matrix contained Al, V, Cr, and Mo elements.

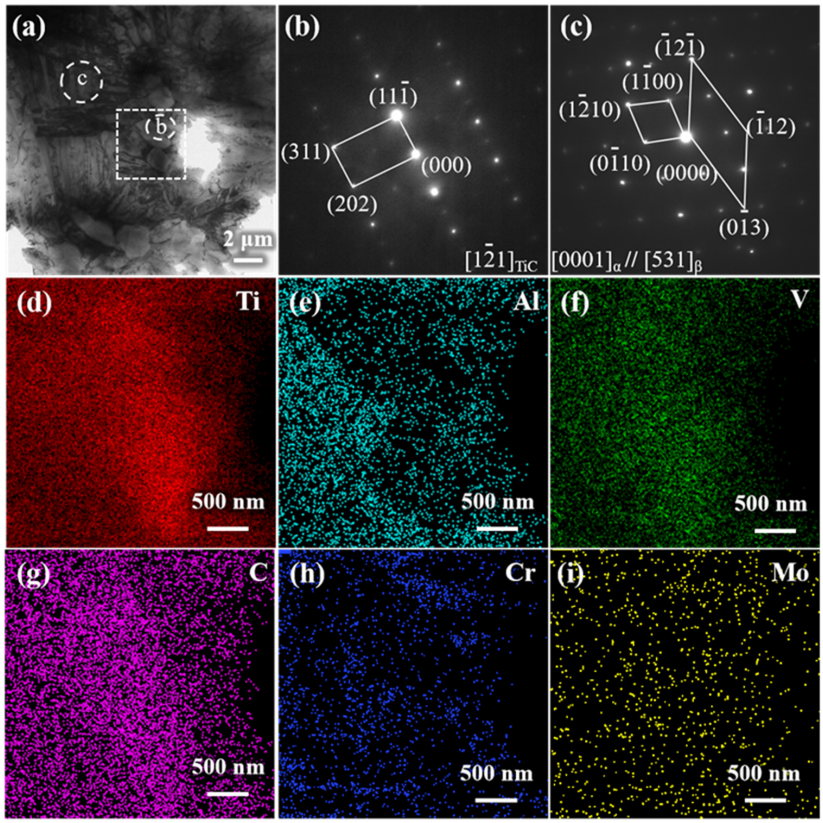

Figure 6. (**a**) TEM bright field image of TMC-20, (**b**,**c**) SAED patterns taken from circle areas in (**a**), (**d**–**i**) EDS images of Ti, Al. V, C, Cr, and Mo in the square area in (**a**).

To investigate the impact of Ti1400 addition on the room-temperature mechanical properties of TMC-0, uniaxial tensile tests were conducted on TMC-5 and TMC-20. Figure 7a presents the engineering stress–strain curves of TMC-5 and TMC-20, as well as TC4 alloy and TMC-0 for comparison. TMC-0, which contained 2.5%TiC, exhibited a yield strength (YS) of 1022 MPa, tensile strength (TS) of 1126 MPa, and total elongation (tEl) of 9.7%. Compared with the TC4 alloy, its the yield strength increased by 20% and the tensile strength increased by 15%, but the elongation decreased by 35%. It is demonstrated that TiC can improve the strength of the composites, but significantly reduces the elongation of the composites. The yield strength of the TMC-5 sample was 1029 MPa and the tensile strength was 1134 MPa. In comparison to TMC-0, TMC-5 did not exhibit significant improvements in yield strength and tensile strength. However, the total elongation (14.0%) was significantly higher than that of TMC-0. It shows that 5 wt% Ti1400 cannot improve the strength of the composites, but it can improve the plasticity of the composites. As the Ti1400 content increased, the yield strength, tensile strength, and total elongation of TMC-20 improved to 1061 MPa, 1178 MPa, and 12.8%, respectively. Compared with the TC4 alloy, its yield strength increased by 25%, tensile strength increased by 20%, and elongation only decreased by 23%. Compared with TMC-0, the tensile strength of TMC-20 increased by 50 MPa and elongation increased by 2%. The tensile strength of TMC-20 was higher than that of TMC-5, and the total elongation was slightly reduced, but still significantly higher than that of TMC-0. This indicates that 20 wt.% Ti1400 can not only improve the strength but also the plasticity of the composites. Figure 7b illustrates the average yield strength, tensile strength, and total elongation of the TC4 alloy and composites. The addition of Ti1400 improved the total elongation of TMC-0 without compromising its tensile strength. By incorporating 20% Ti1400 content, the composite exhibited a significant improvement in both strength and ductility, offering a viable solution to the issue of decreased ductility in ceramic phase reinforced composites.

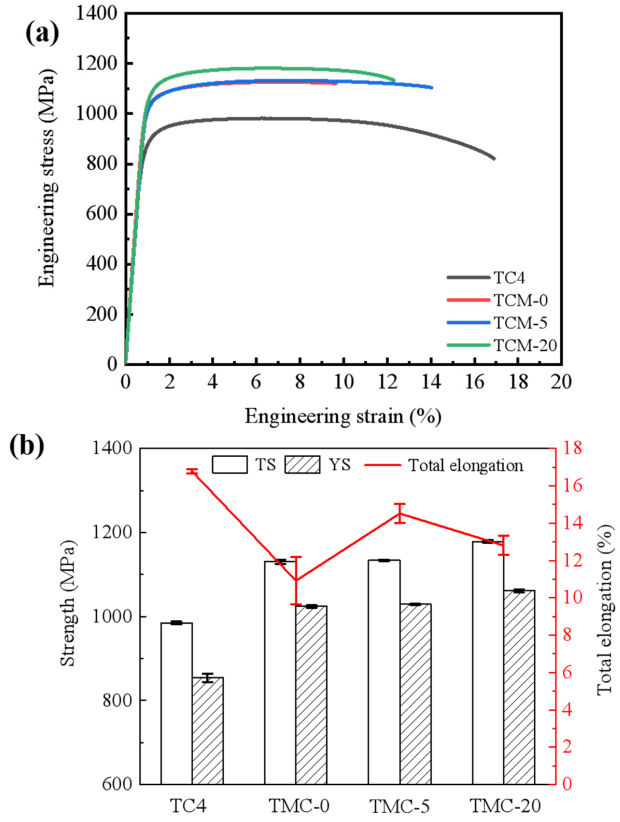

Figure 7. (**a**) Engineering stress–strain curves of TC4 alloy and the composites with different Ti1400 alloy contents, (**b**) the yield strength (YS), tensile strength (TS), and total elongation (tEl) of TC4 alloy and composites.

4. Discussion

The findings of this study indicate that TMC-20 exhibits outstanding mechanical properties. In comparison to TMC-0, the inclusion of Ti1400 alloy not only enhances its strength, but also significantly elevates its overall elongation. The enhancement of both strength and ductility can be attributed not only to the refinement of grains induced by TiC and Ti1400 alloy, but also to the favorable changes in composition and structure between Ti1400 alloy and the TC4 matrix, as well as the strong interface bonding between them.

In general, the strength of a material is heavily influenced by its internal grain size. According to the Hall–Petch equation [40], the strength of materials increases as the grain size decreases. For the 2.5%TiC/TC4 composite (TMC-0), the in situ TiC particles were dispersed in a discontinuous network structure within the TC4 matrix, which restricted the development of lamellar structures and led to a significant reduction in grain size, as illustrated in Figure 4. According to statistics, the average grain sizes of TC4 alloy and TMC-0 were 71.6 μm and 32.53 μm, respectively, indicating that the addition of reinforcement can significantly reduce the grain size of the material. In addition, micron-scale TiC particles with ultra-high strength are capable of severely limiting dislocation motion, which also plays a role in enhancing the strength [41]. However, the dislocation will seriously accumulate around the TiC particles, resulting in serious stress concentration, which provides favorable conditions for the formation and propagation of microcracks, leading to premature fracture, and reducing the total elongation of the materials. Therefore, relieving the stress concentration near the reinforcements is the key to improving ductility.

Concerning the (Ti1400 + TiC)/TC4 composites (TMC-5 and TMC-20), the reduced grain size within the Ti1400 regions and the solid solution strengthening of Cr and Mo elements [42,43] confer a higher strength to the Ti1400 region compared to the TC4 matrix. Hence, the added Ti1400 alloy can also function as a reinforcement. As a result of the substitutional elements' (Cr and Mo) diffusion and the gradual narrowing of the lamellar microstructures, a transition zone emerged between the Ti1400 region and the TC4 matrix. Due to the diffusion of elements, there is a continuous change in the microstructure. The closer to the Ti1400 region, the narrower the lamellar α phase, and the spacing between α phases also decreases. As a result, the α/β interfaces increase, making it increasingly difficult for dislocations to move towards the Ti1400 region, resulting in a significant increase in its strength [44–46]. Such reinforcement effect gradually shows up with the increase in Ti1400 alloy content. Moreover, the usefulness of Ti1400 alloy is more evident in enhancing ductility. In contrast to TiC particles, the presence of a transition zone enables Ti1400 alloy to form a superior interface with the TC4 matrix. Consequently, the uneven distribution of Ti1400 alloy within the matrix can alleviate severe stress concentration, leading to a more even stress distribution in the composite and preventing premature fracture. The EBSD characterization was performed on the tensile fracture samples of the (20%Ti1400 + 0.25%TiC)/Ti1400 composite (TMC-20). In the EBSD phase figure (Figure 8a), the organization in the Ti1400 region is mainly composed of laminar β phase, with the β phase gradually decreasing from the Ti1400 region to the TC4 matrix. The α/β interface in the transition region is significantly increased. The organization in the TC4 matrix is mainly composed of laminar α phase. TiC particles with relatively large hardness can cause dislocation pile-ups, which mainly occur in the TC4 matrix and are rarely found in the Ti1400 region and transition zone. Therefore, the change in the β phase and the increase in the α/β interface in the Ti1400 region and transition zone make the resistance of dislocation motion uniformly distributed and continuously increased, which is not only conducive to the increase of strength but also more conducive to the improvement of elongation. As shown in the EBSD kernel average misorientation (KAM) map of Figure 8b, different colors represent different KAM, in which red indicates the maximum misorientation. There is a certain relationship between the KAM and the Geometrically Necessary Dislocation (GND) density. A larger KAM value implies a higher GND density. In the tensile fracture samples, the KAM value of the β phase in the TC4 matrix is significantly higher than that of the α phase, and the KAM value near the α/β interface and TiC is larger, indicating a greater

stress concentration near the α/β interface and TiC. This provides favorable conditions for crack formation and propagation, leading to a reduction in elongation and toughness. In the transition zone and Ti1400 region, the KAM value of the α/β interface is lower than the maximum KAM value of the α/β interface in the TC4 matrix, and the KAM value distribution is relatively uniform, which partially alleviates stress concentration. Moreover, the KAM value of the β phase is significantly higher than that of the α phase, proving that deformation mainly occurs in the β phase, and an increase in the volume fraction of the β phase is beneficial to improve the elongation of the material. As depicted in Figure 9a,b, microcracks were observed in the vicinity of TiC particles and they coalesced and propagated along the TiC particles, ultimately causing the composite to fracture. In contrast, no microcracks were detected around Ti1400 alloy as reinforcement. Furthermore, as depicted in Figure 9, the interface and transition zone between Ti1400 and TC4 remained intact without debonding or cracking after being subjected to stretching, thereby affirming the presence of good interfacial bonding at the Ti1400-TC4 junction. Similar research results have also confirmed that the interfacial strength between metals or alloys is generally higher than that between metals or alloys and ceramic phases. [30] Thus, Ti1400 alloy, as a reinforcement with excellent interfacial bonding with the matrix, significantly enhances the composite's strength, especially in terms of ductility improvement. This low-cost and flexible approach offers a feasible solution to overcome the tradeoff between strength and ductility of composites.

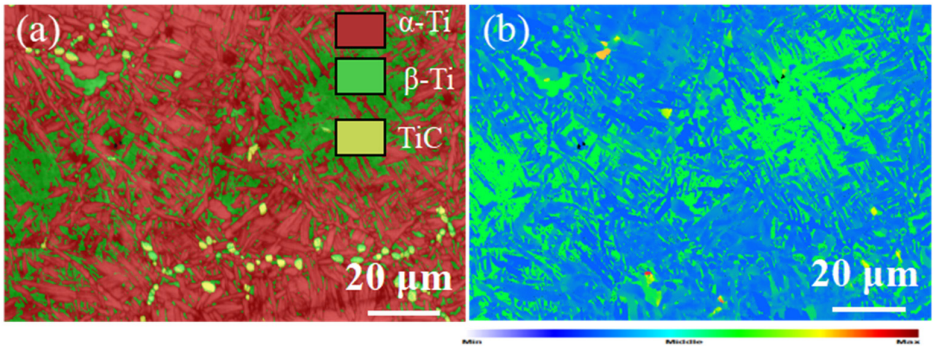

Figure 8. EBSD maps of tensile fracture samples of TMC-20: (**a**) phase figure, (**b**) KAM map.

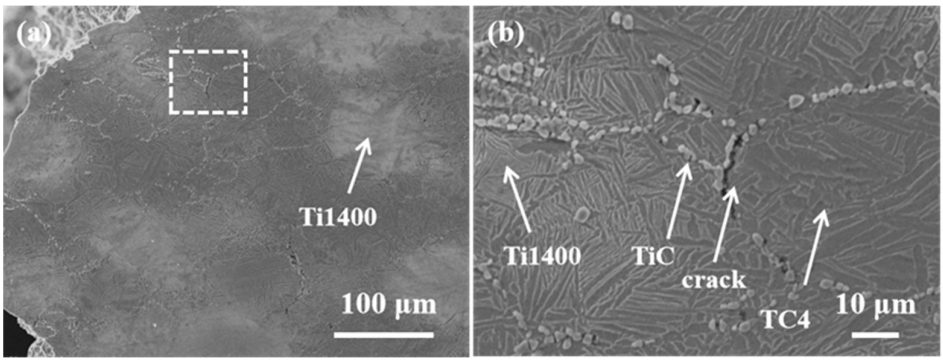

Figure 9. (**a**) SEM image of cross section near the fracture in TMC-20 and (**b**) the magnification SEM image of the square area in (**a**).

5. Conclusions

In this study, the composites with different Ti1400 alloy contents and TC4 alloy were fabricated by spark plasma sintering to explore the microstructures and mechanical properties of the composites. The composites were characterized using SEM, TEM, EPMA, and a tensile test at room temperature. The strengthening mechanism was also analyzed, and the primary findings are summarized below.

(1) The microstructures of (Ti1400 + TiC)/TC4 composites exhibited discontinuous distribution of in situ-formed TiC particles, forming a network structure. The compositional and structural transition zone between the Ti1400 alloy and TC4 matrix were crucial in achieving superior mechanical properties.
(2) The yield strength and tensile strength of the TiC/TC4 composite were substantially higher than those of the TC4 alloy. However, the total elongation was only 57% of that in the TC4 alloy. Increasing the Ti1400 alloy content enhanced the tensile strength of the composite while still maintaining a significantly higher total elongation compared to the TiC/TC4 composite.
(3) The increase in strength mainly came from the additional solid solution strengthening provided by the substitutional elements Cr and Mo and the fine grain strengthening. The compositional and structural transition zone formed by element diffusion had a better interface combination between the Ti1400 alloy and TC4 matrix, which can alleviate the severe stress concentration and is conducive to the improvement of elongation.

Author Contributions: Conceptualization, Y.Z. and M.L. (Mingyang Li); methodology, G.S.; software, N.H.; validation, N.H., L.D. and M.L.; formal analysis, N.H.; investigation, L.D.; resources, Y.Z.; data curation, N.H.; writing—original draft preparation, N.H.; writing—review and editing, M.L. (Mingjia Li); visualization, M.L. (Mingyang Li); supervision, J.X.; project administration, Y.Z.; funding acquisition, Y.Z. All authors have read and agreed to the published version of the manuscript.

Funding: This work was financially supported by the National Natural Science Foundation of China, China (No. 52271138), Natural Science Basic Research Plan in Shaanxi Province of China (No. 2022JQ-437), Key Research and Development Projects of Shaanxi Province (No. 2023-YBGY-433) and National Program for Introduction of Foreign Experts (No. G2022041019L).

Institutional Review Board Statement: Not applicable.

Informed Consent Statement: Not applicable.

Data Availability Statement: Data sharing is not applicable to this article.

Conflicts of Interest: The authors declare no conflict of interest.

References

1. Shang, C.; Zhang, F.; Xiong, Y.; Wan, Q.; Chen, F. Spark Plasma Forging and Network Size Effect on Strength-Ductility Trade-off in Graphene Reinforced Ti6Al4V Matrix Nanocomposites. *Mater. Sci. Eng. A* **2023**, *862*, 144480. [CrossRef]
2. Ghasali, E.; Ghahremani, D.; Orooji, Y. Using metallic additives as a bonding layer to produce Ti-based laminated composites via spark plasma sintering. *J. Sci. Adv. Mater. Devices* **2021**, *6*, 435–445. [CrossRef]
3. Wang, H.; Zhang, H.M.; Cheng, X.W.; Chang, S.; Mu, X.N. Effect of Ball Milling Time on Microstructure and Mechanical Properties of Graphene Nanoplates and TiBw Reinforced Ti–6Al–4V Alloy Composites. *Mater. Sci. Eng. A* **2022**, *861*, 144240. [CrossRef]
4. Chang, S.; Du, W.; Zhao, Z.; Bai, P. Microstructure and High Temperature-Mechanical Properties of TiC/Graphene/Ti6Al4V Composite Formed by Laser Powder Bed Fusion. *Metals* **2023**, *13*, 163. [CrossRef]
5. Dong, L.; Lu, J.; Fu, Y.; Huo, W.; Liu, Y.; Li, D.; Zhang, Y. Carbonaceous nanomaterial reinforced Ti-6Al-4V matrix composites: Properties, interfacial structures and strengthening mechanisms. *Carbon* **2020**, *164*, 272–286. [CrossRef]
6. Wang, S.; Huang, L.; Jiang, S.; Zhang, R.; Liu, B.; Sun, F.; An, Q.; Jiao, Y.; Geng, L. Microstructure evolution and tensile properties of as-rolled TiB/TA15 composites with network microstructure. *Mater. Sci. Eng. A* **2021**, *804*, 140783. [CrossRef]
7. Wu, H.; Li, S.; Han, Y.; Huang, G.; Mao, J.; Lu, W. Understanding the confined TiB fiber-like structure for strength-ductility combination of discontinuous-reinforced titanium matrix composites. *Mater. Sci. Eng. A* **2022**, *852*, 143645. [CrossRef]
8. Zhang, F.; Wang, J.; Liu, T.; Shang, C. Enhanced Mechanical Properties of Few-Layer Graphene Reinforced Titanium Alloy Matrix Nanocomposites with a Network Architecture. *Mater. Des.* **2020**, *186*, 108330. [CrossRef]
9. Tjong, S.C.; Mai, Y.-W. Processing-structure-property aspects of particulate and whisker-reinforced titanium matrix composites. *Compos. Sci. Technol.* **2008**, *68*, 583–601. [CrossRef]
10. Chen, R.; An, Q.; Wang, S.; Huang, L.; Zhang, R.; Wang, C.; Zhou, S.; Geng, L. Overcoming the Strength-Ductility Trade-off Dilemma in TiBw/TC18 Composites via Network Architecture with Trace Reinforcement. *Mater. Sci. Eng. A* **2022**, *842*, 143092. [CrossRef]
11. Zhang, R.; Wang, S.; Chen, X.; An, Q.; Huang, L.; Geng, L.; Yang, F. Significantly Enhanced Superplasticity of TiBw/near-α Ti Composite: Microstructure Tailoring and Deformation Mechanisms. *Mater. Sci. Eng. A* **2022**, *853*, 143772. [CrossRef]

12. Lin, F.; Ren, M.; Jia, F.; Huo, M.; Yang, M.; Chen, Z.; Jiang, Z. Achieving Balanced Strength-Ductility of Heterostructured TiC/Graphene Nanoplatelets (GNPs) Reinforced Al Matrix Composites by Tuning TiC-to-GNPs Ratio. *Compos. Commun.* **2023**, *38*, 101529. [CrossRef]
13. Ge, Y.; Zhang, H.; Cheng, X.; Fan, Q.; Zhang, Z.; Mu, X.; Liu, L.; Feng, K. Achieving High Performance in ($NiTi_2$ + TiC)/Ti Composites with Network Architecture via Reaction Interface Design. *J. Alloys Compd.* **2022**, *925*, 166230. [CrossRef]
14. Moradi, M.; Moazeni, M.; Salimijazi, H.R. Microstructural characterization and failure mechanism of vacuum plasma sprayed Ti-6Al-4V/B4C composite. *Vacuum* **2014**, *107*, 34–40. [CrossRef]
15. Liu, Z.; Gao, B.; Liu, Y.; Ji, S.; Ao, Q. Research on Preparation and Characterization of Ti-Ti5Si3 Gradient Composite Porous Material via in-Situ Reactive Process. *J. Alloys Compd.* **2022**, *899*, 163405. [CrossRef]
16. Ghasali, E.; Nezhad, M.S.A.; Ghazvinian, S. Preparation of Ti-based laminated composites through spark plasma sintering with different carbon sources as the bonding layer. *Ceram. Int.* **2019**, *45*, 14045–14057. [CrossRef]
17. Yue, H.; Peng, H.; Fan, G.; Yang, J.; Chen, H.; Fang, X. Microstructure and Mechanical Properties of Y2O3-Bearing Ti–48Al–2Cr–2Nb Alloy Prepared by Selective Electron Beam Melting. *Mater. Sci. Eng. A* **2022**, *840*, 142960. [CrossRef]
18. Singh, H.; Hayat, M.; He, Z.; Peterson, V.K.; Das, R.; Cao, P. In situ neutron diffraction observations of Ti-TiB composites. *Compos. Part A* **2019**, *124*, 105501. [CrossRef]
19. Jiang, B.; Wang, L.; Yan, H.; Zhu, G.; Teng, J.; Wang, B.; Luo, L.; Chen, R.; Su, Y.; Guo, J. Hydrogen-Induced Modification of the Interface between Matrix and Ceramic Phase of (TiB + TiC)/Ti–6Al–4V. *Compos. Commun.* **2023**, *37*, 101434. [CrossRef]
20. Wang, Y.; Zhu, M.; Dong, L.; Sun, G.; Zhang, W.; Xue, H.; Fu, Y.; Elmarakbi, A.; Zhang, Y. In-Situ Synthesized TiC/Ti-6Al-4V Composites by Elemental Powder Mixing and Spark Plasma Sintering: Microstructural Evolution and Mechanical Properties. *J. Alloys Compd.* **2023**, *947*, 169557. [CrossRef]
21. Wang, J.; Guo, X.; Qin, J.; Zhang, D.; Lu, W. Microstructure and mechanical properties of investment casted titanium matrix composites with B4C additions. *Mater. Sci. Eng. A* **2015**, *628*, 366–373. [CrossRef]
22. Moghadam, A.D.; Omrani, E.; Menezes, P.L.; Rohatgi, P.K. Mechanical and tribological properties of self-lubricating metal matrix nanocomposites reinforced by carbon nanotubes (CNTs) and graphene-a review. *Compos. B Eng.* **2015**, *77*, 402–420. [CrossRef]
23. Sun, G.; Zhuang, S.; Jia, D.; Pan, X.; Sun, Y.; Tu, F.; Lu, M. Facile Fabricating Titanium/Graphene Composite with Enhanced Conductivity. *Mater. Lett.* **2023**, *333*, 133680. [CrossRef]
24. Lu, J.; Dong, L.; Liu, Y.; Fu, Y.; Zhang, W.; Du, Y.; Zhang, Y.; Zhao, Y. Simultaneously enhancing the strength and ductility in titanium matrix composites via discontinuous network structure. *Compos. Part A* **2020**, *136*, 105971. [CrossRef]
25. Cho, S.; Kim, J.; Jo, I.; Park, J.H.; Lee, J.; Hong, H.-U.; Lee, B.H.; Hwang, W.R.; Suh, D.-W.; Lee, S.-K. Effect of molybdenum on interfacial properties of titanium carbide reinforced Fe composite. *J. Mater. Sci. Technol.* **2022**, *107*, 252–258. [CrossRef]
26. Tan, C.; Liu, Y.; Weng, F.; Ng, F.L.; Su, J.; Xu, Z.; Ngai, X.D.; Chew, Y. Additive manufacturing of voxelized heterostructured materials with hierarchical phases. *Addit. Manuf.* **2022**, *54*, 102775. [CrossRef]
27. Wimler, D.; Lindemann, J.; Gammer, C.; Spoerk-Erdely, P.; Stark, A.; Clemens, H.; Mayer, S. Novel intermetallic-reinforced near-α Ti alloys manufactured by spark plasma sintering. *Mater. Sci. Eng. A* **2020**, *792*, 139798. [CrossRef]
28. Yu, H.; Sun, Y.; Hu, L.; Zhou, H.; Wan, Z. Microstructural evolution of AZ61-10 at.%Ti composite powders during mechanical milling. *Mater. Des.* **2016**, *104*, 265–275. [CrossRef]
29. Luo, H.; Li, J.; Ye, J.; Lu, Y.; Tan, J.; Song, J.; Chen, X.; Zheng, K.; Pan, F. Influence of Ti-6Al-4V particles on the interfacial microstructure and strength-ductility synergetic mechanism of AZ91 magnesium alloy. *Mater. Charact.* **2022**, *191*, 112154. [CrossRef]
30. Xiong, Y.; Zhang, F.; Huang, Y.; Shang, C.; Wan, Q. Multiple strengthening via high-entropy alloy particle addition in titanium matrix composites fabricated by spark plasma sintering. *Mater. Sci. Eng. A* **2022**, *859*, 144235. [CrossRef]
31. Ma, G.; Liu, X.; Song, C.; Niu, F.; Wu, D. TiCp reinforced Ti6Al4V of follow-up synchronous electromagnetic induction-laser hybrid directed energy deposition: Microstructure evolution and mechanical properties. *Addit. Manuf.* **2022**, *59*, 103087. [CrossRef]
32. Jayaprakash, M.; Ping, D.H.; Yamabe-Mitarai, Y. Effect of Zr and Si addition on high temperature mechanical properties of near-α Ti–Al–Zr–Sn based alloys. *Mater. Sci. Eng. A* **2014**, *612*, 456–461. [CrossRef]
33. Jiang, X.J.; Zhou, Y.K.; Feng, Z.H.; Xia, C.Q.; Tan, C.L.; Liang, S.X.; Zhang, X.Y.; Ma, M.Z.; Liu, R.P. Influence of Zr content on β-phase stability in α-type Ti–Al alloys. *Mater. Sci. Eng. A* **2015**, *639*, 407–411. [CrossRef]
34. Vidyuk, T.M.; Dudina, D.V.; Korchagin, M.A.; Gavrilov, A.I.; Skripkina, T.S.; Ukhina, A.V.; Anisimov, A.G.; Bokhonov, B.B. Melting at the inter-particle contacts during Spark Plasma Sintering: Direct microstructural evidence and relation to particle morphology. *Vacuum* **2020**, *181*, 109566. [CrossRef]
35. Feng, T.; Zheng, W.; Chen, W.; Shi, Y.; Fu, Y.Q. Enhanced interfacial wettability and mechanical properties of Ni@Al_2O_3/Cu ceramic matrix composites using spark plasma sintering of Ni coated Al_2O_3 powders. *Vacuum* **2021**, *184*, 109938. [CrossRef]
36. Liu, C.; Lu, W.; Xia, W.; Du, C.; Rao, Z.; Best, J.P.; Brinckmann, S.; Lu, J.; Gault, B.; Dehm, G.; et al. Massive interstitial solid solution alloys achieve near-theoretical strength. *Nat. Commun.* **2022**, *13*, 1102. [CrossRef]
37. Zhang, S.; Liu, J.; Zhao, Q.; Zhang, C.; Bolzoni, L.; Yang, F. Microstructure characterization of a high strength Ti–6Al–4V alloy prepared from a powder mixture of TiH2 and 60Al40V masteralloy powders. *J. Alloys Compd.* **2020**, *818*, 152815. [CrossRef]
38. Suzuki, T.; Takeuchi, S.; Yoshinaga, H. *Dislocation Dynamics and Plasticity*; Springer: Berlin, Germany, 1991.

39. Zhu, L.; Zhang, Q.; Chen, Z.; Wei, C.; Cai, G.-M.; Jiang, L.; Jin, Z.; Zhao, J.-C. Measurement of interdiffusion and impurity diffusion coefficients in the bcc phase of the Ti–X (X = Cr, Hf, Mo, Nb, V, Zr) binary systems using diffusion múltiples. *J. Mater. Sci.* **2016**, *52*, 3255–3268. [CrossRef]
40. Hansen, N. Hall-Petch relation and boundary strengthening. *Scr. Mater.* **2004**, *51*, 801–806. [CrossRef]
41. Zhang, B.; Zhang, F.; Saba, F.; Shang, C. Graphene-TiC hybrid reinforced titanium matrix composites with 3D network architecture: Fabrication, microstructure and mechanical properties. *J. Alloys Compd.* **2021**, *859*, 157777. [CrossRef]
42. Jiang, S.; An, Q.; Cui, X.; Xiang, X.; Huang, L.; Zhang, R.; Sun, Y.; Geng, L. Fabrication and mechanical properties of the titanium matrix composites based on Ti6Al4V-ZrB_2-(Si) system. *Mater. Sci. Eng. A* **2021**, *819*, 141488. [CrossRef]
43. Zhang, T.; Huang, Z.; Yang, T.; Kong, H.; Luan, J.; Wang, A.; Wang, D.; Kuo, W.; Wang, Y.; Liu, C.T. In situ design of advanced titanium alloy with concentration modulations by additive manufacturing. *Science* **2021**, *374*, 478–482. [CrossRef] [PubMed]
44. Zhao, Q.; Sun, Q.; Xin, S.; Chen, Y.; Wu, C.; Wang, H.; Xu, J.; Wan, M.; Zeng, W.; Zhao, Y. High-strength titanium alloys for aerospace engineering applications: A review on melting-forging process. *Mater. Sci. Eng. A* **2022**, *845*, 143260. [CrossRef]
45. Froes, F.H.; Bomberger, H.B. The beta titanium alloys. *JOM* **1985**, *37*, 28–37. [CrossRef]
46. Ankem, S.; Margolin, H.; Greene, C.A.; Neuberger, B.W.; Oberson, P.G. Mechanical properties of alloys consisting of two ductile phases. *Prog. Mater. Sci.* **2006**, *51*, 632–709. [CrossRef]